THE JOURNAL OF PHYSICAL CHEMISTRY A
A JOURNAL OF THE AMERICAN CHEMICAL SOCIETY

pubs.acs.org/JPCA Article

Photoelectron Spectroscopic and *ab Initio* Computational Studies of the Anion, $HThO^-$

Mary Marshall, Zhaoguo Zhu, Junzi Liu, Lan Cheng,* and Kit H. Bowen*

Cite This: *J. Phys. Chem. A* 2021, 125, 1903–1909 Read Online

ACCESS | Metrics & More | Article Recommendations

ABSTRACT: The synergetic combination of anion photoelectron spectroscopy and high-level relativistic coupled-cluster calculations was employed to study the anion, $HThO^-$. The atomic connectivity of this anion was found to be $HThO^-$ and not $ThOH^-$. Vibrational and electronic energy spacings in the $HThO^-$ photoelectron spectrum were measured and calculated, with good agreement between them being found. Computations yielded electronic energies and equilibrium structures as well as enabling orbital analyses. The adiabatic electron affinity (EA_a) of HThO was determined to be 1.297 ± 0.035 eV.

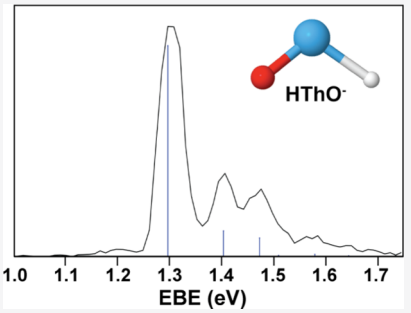

INTRODUCTION

Nuclear energy offers a high-energy-density alternative to greenhouse gas-emitting fossil fuels; however, radiological waste disposal and proliferation risks remain as significant issues. Currently, most nuclear reactors utilize isotopically enriched uranium-235 as their fuel, but the possibility of instead using thorium as the fuel has attracted attention.[1−4] This is largely because thorium is over three times more abundant than uranium, and thorium reactors are reputed to be safer to operate, to produce less radioactive waste, and to have a reduced proliferation threat. Thorium reactors are inherently breeder reactors, converting natural, non-fissile thorium-232 (with the aid of neutrons provided by a seeded fissile material, e.g., uranium-235 or plutonium-239) into the fissile isotopes, uranium-233 and uranium-232. Therefore, thorium reactors are comparable to uranium breeder reactors, which convert uranium-238 into fissile plutonium-239. In these, as well as in all nuclear reactors, fission results in heat, which in turn is used to generate electricity.

Thorium is the only actinide element not to possess 5f electrons in its atomic ground state. Due to its $[Rn]6d^27s^2$ electronic configuration, thorium is normally present in its tetravalent state. In aqueous solutions, for example, thorium forms numerous hydroxides, such as, $Th(OH)_3^+$, $Th(OH)_2^{2+}$, $Th(OH)^{3+}$, and $Th_2(OH)_2^{6+}$.[5−10] However, in matrix isolation studies, where laser-ablated thorium atoms and water molecules were co-deposited on an argon ice, HTh(OH) and HThO were found to be the major intermediates and reaction products, with only residual amounts of H_2ThO, $HThO(OH)$, $HTh(OH)_3$, and $OTh(OH)_2$ detected. Interestingly, there was no evidence of thorium hydroxide, ThOH, having been formed. The formation of the intermediate, [HTh(OH)]*, (see reaction 1) was favored over the direct dissociation of water (see reaction 2).[11]

$$Th + H_2O \rightarrow [HTh(OH)]^* \rightarrow H + HThO \quad (1)$$

$$Th + H_2O \rightarrow H + ThOH \quad (2)$$

The same result was found when reacting Th atoms with a H_2/O_2 mixture.[11] The reaction of thorium atoms with hydrogen peroxide generated $Th(OH)_2$ and $Th(OH)_4$, but it did not yield ThOH.[12] Water activation was also observed in guided ion beam studies, where Th^+ cations reacted with D_2O to form $DThO^+$.[13] Several Fourier transform ion cyclotron resonance mass spectrometric studies had reported the reactions of Th^+ and Th^{2+} with H_2O to form ThO^+ and $ThOH^+$.[14−16] However, subsequent calculations found these reactions preferred $HThO^{+/2+}$ over the $ThOH^{+/2+}$ isomer.[17]

The reaction of thorium atoms with water or with hydrogen/oxygen mixtures differs significantly from that of the other actinides. Based on density-functional theory (DFT) calculations, the reaction between U^+ and water favors the dehydration product, UO^+, although small amounts of UOH^+ are also predicted to be formed.[18] Uranium metal exhibits a highly exothermic reaction with water, generating uranium hydride as an intermediate before yielding the final UO_2 product.[19] Plutonium metal reacts with water to produce

Received: December 28, 2020
Revised: February 5, 2021
Published: March 1, 2021

https://dx.doi.org/10.1021/acs.jpca.0c11539
J. Phys. Chem. A 2021, 125, 1903−1909

PuOH and H_2, although, upon heating, these initial products react to yield PuO_2 and PuH_2.[20] Thus, while HThO is the favored product of Th + H_2O reactions, HMO has not been observed as the reaction product of other actinides (M) with water. The HM'O stoichiometry is, however, a known product of reactions between group IV metals (M') and water. Matrix infrared spectroscopic studies showed that TiO_2 reacting with H_2O formed HTiO, although the main product was OTi-$(OH)_2$.[21] The formation of HThO as a product of the Th + H_2O reaction underscores thorium's kinship with the group IV transition metals, both because of its four valence electrons and its lack of f-electrons.

In the present work, we utilized anion photoelectron spectroscopy (PES) in synergetic conjunction with high-level relativistic coupled-cluster calculations, finding the principal thorium-containing anionic species observed to be $HThO^-$ and not $ThOH^-$. We then measured and calculated both the electron affinity of HThO and the energy separations between the ground state of neutral HThO and its low-lying electronically excited states.

METHODS

Experimental Section. Anion PES is conducted by crossing a mass-selected anion beam with a fixed energy photon beam and energy analyzing the resulting photodetached electrons. The photodetachment process is governed by the energy conserving relationship, $h\nu$ = EBE + EKE, where $h\nu$ is the photon energy, EBE is the electron binding (photodetachment transition) energy, and EKE is the electron kinetic energy. Our photoelectron apparatus has been described previously.[22] Briefly, it consists of an ion source, a time-of-flight mass spectrometer, a Nd:YAG photodetachment laser, and a magnetic bottle electron energy analyzer. The second (532 nm, 2.33 eV), third (355 nm, 3.49 eV), and fourth (266 nm, 4.66 eV) harmonics of an Nd:YAG laser were used to photodetach the $HThO^-$ anion. The resolution of the energy analyzer is ~35 meV at EKE = 1 eV. Photoelectron spectra were calibrated against the well-known transitions of Cu^-.[23] The $HThO^-$ anions were generated in a laser vaporization ion source. A translating, rotating, surface-oxidized thorium rod was ablated using the second harmonic photon energy of a different Nd:YAG laser (532 nm, 2.33 eV), while 20 psi of UHP H_2 gas expanded over the rod.

Computational. All calculations were performed using the CFOUR program package.[24−30] Equilibrium structures for the ground state ($1^1A'$) and the first excited state ($1^3A''$) of the $HThO^-$ anion were calculated using coupled-cluster singles and doubles with noniterative triples [CCSD(T)][31] method. Throughout our calculations, scalar-relativistic effects were taken into account using the spin-free exact two-component theory in its one-electron variant (SFX2C-1e)[32,33] and correlation-consistent triple-zeta basis sets (cc-pVTZ)[34,35] recontracted for the SFX2C-1e scheme. Th 1s, 2s, 2p, 3s, 3p, 3d, 4f, 4p, 4d, 4f, 5s, 5p, 5d electrons and O 1s electrons were frozen in all CC calculations. The equilibrium structure for the electronic ground state ($1^2A'$) of the neutral HThO molecule was also obtained at the SFX2C-1e-CCSD(T)/cc-pVTZ level. The equation-of-motion electron attachment coupled-cluster singles and doubles (EOMEA-CCSD)[36] method was used to obtain the equilibrium structures for three electronically excited states of HThO, namely, the $1^2A''$, $2^2A'$, and $2^2A''$ states. For comparison, we also carried out a geometry optimization for the electronic ground state, $X^2\Delta$, of ThOH. Geometry optimizations performed here exploited the availability of analytic gradients for the SFX2C-1e scheme[28] and the coupled-cluster methods.[26,27] Table 1 presents the electron configurations of these six states as well as the vertical electronic energies between them and the electronic ground state of the $HThO^-$ anion in its equilibrium geometry.

Table 1. Electron Configurations of Low-Lying Electronic States of $HThO^-$ and HThO as Well as Their Vertical Electronic Energies Relative to the Electronic Ground State of the $HThO^-$ Anion, $1^1A'$, in Its Equilibrium Geometry. The Valence Molecular Orbitals Shown Here Comprise Th 6s, 6p, 6d, 7s, O 2s, 2p, and H 1s Orbitals

	leading electron configuration	vertical electronic energy (eV)
$HThO^-$ $1^1A'$	$1a'^2 2a'^2 3a'^2 1a''^2 4a'^2 5a'^2 2a''^2 6a'^2 7a'^2 8a'^2$	0
$HThO^-$ $1^3A''$	$1a'^2 2a'^2 3a'^2 1a''^2 4a'^2 5a'^2 2a''^2 6a'^2 7a'^2 8a'^1 3a''^1$	0.73
HThO $1^2A'$	$1a'^2 2a'^2 3a'^2 1a''^2 4a'^2 5a'^2 2a''^2 6a'^2 7a'^2 8a'^1$	1.27
HThO $1^2A''$	$1a'^2 2a'^2 3a'^2 1a''^2 4a'^2 5a'^2 2a''^2 6a'^2 7a'^2 3a''^1$	2.15
HThO $2^2A'$	$1a'^2 2a'^2 3a'^2 1a''^2 4a'^2 5a'^2 2a''^2 6a'^2 7a'^2 9a'^1$	2.47
HThO $2^2A''$	$1a'^2 2a'^2 3a'^2 1a''^2 4a'^2 5a'^2 2a''^2 6a'^2 7a'^2 4a''^1$	2.85

In the present calculations, the electronic energies of the $1^3A''$ state of $HThO^-$ and the $1^2A'$ state of HThO relative to the $1^1A'$ state of $HThO^-$ were calculated as the difference of the corresponding SFX2C-1e-CCSD(T)/cc-pVTZ energies. The electronic energies of the $1^2A''$, $2^2A'$, and $2^2A''$ states of HThO relative to the $1^1A'$ state of $HThO^-$ were obtained using an indirect scheme. We computed the difference between SFX2C-1e-EOMEA-CCSD/cc-pVTZ energies of these three states and that for the $1^2A'$ state of HThO and then added the CCSD(T) relative energy between the HThO $1^2A'$ state and the $HThO^-$ $1^1A'$ state.

A Franck−Condon (FC) simulation was also carried out to obtain the vibrational progression for the $HThO^-$ $1^1A' \rightarrow$ HThO $1^2A'$ transition. The harmonic vibrational frequencies and normal coordinates of the $HThO^-$ $1^1A'$ state were obtained by means of numerical differentiation[29] of analytic SFX2C-1e-CCSD(T)/cc-pVTZ gradients. The potential energy surface of the HThO $1^2A'$ state was then represented as a Taylor expansion using the equilibrium structure of the $HThO^-$ $1^1A'$ state as the origin, in which SFX2C-1e-CCSD(T)/cc-pVTZ energies in 125 grid points were fit into a quartic function of displacements in terms of the normal coordinates of the $HThO^-$ $1^1A'$ state. The vibrational Schrödinger equation was solved on this potential energy surface using products of harmonic oscillator functions of the $HThO^-$ $1^1A'$ state as basis functions to represent the vibrational wave functions.[30] The FC overlap integrals with the vibrational ground state of the $HThO^-$ $1^1A'$ state were then obtained in a straightforward manner.

RESULTS

Together with H_2, the residual oxygen on the thorium rod introduced enough oxygen into the system to produce $HThO^-$. The resulting mass spectrum is presented in Figure 1. The dominant peak at mass 249 amu is $HThO^-$. It was

https://dx.doi.org/10.1021/acs.jpca.0c11539
J. Phys. Chem. A 2021, 125, 1903−1909

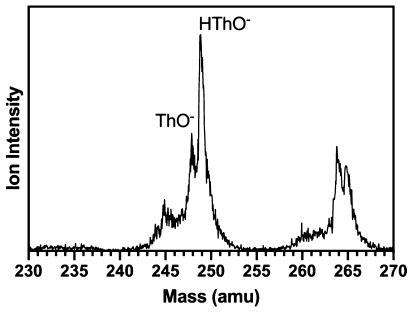

Figure 1. Mass spectrum obtained by expanding H_2 gas over a laser ablated thorium rod. The peak at 249 amu corresponds to the $HThO^-$ anion.

present only when H_2 was utilized as the expansion gas. The mass peak at 248 amu is ThO^-. Both ThO^- and ThO_2^- were observed with no expansion gas and with H_2 as the expansion gas, but $HThO^-$ and $HThO_2^-$ were only seen when H_2 was employed.

Figure 2 presents the photoelectron spectra of $HThO^-$, that is, the anion at mass 249 amu. These were collected using the

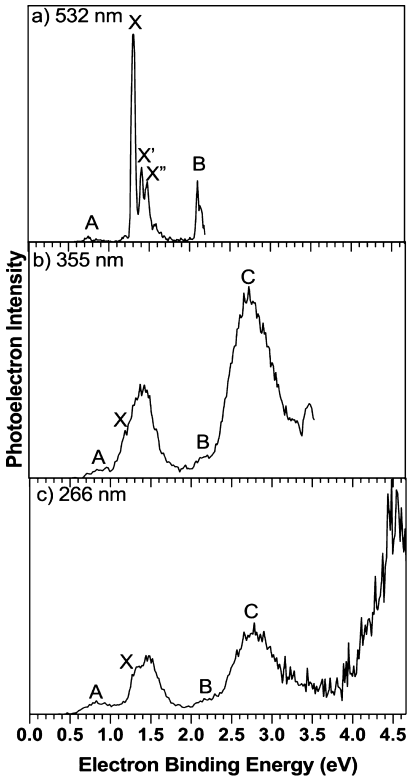

Figure 2. The photoelectron spectra of the anion $HThO^-$ collected using (a) 532 nm, (b) 355 nm, and (c) 266 nm wavelength photons.

532, 355, and 266 nm wavelengths of the Nd:YAG photodetachment laser. The EBEs corresponding to various peak positions are listed in Table 2. The peak positions taken from Figure 2a are the EBE values of the intensity maxima of peaks A, X, X′, X″, and B. The peak positions for spectral feature, X, in Figure 2 b,c are approximate origin transition EBE values. These estimates have accounted for their vibrational progression profiles. The peak positions for features, B and C, in Figure 2 b,c are the EBE values of their intensity maxima.

Table 2. Electron Binding Energy (eV) Values of the Observed Transitions in the Photoelectron Spectra of $HThO^-$

	electron binding energy (eV)		
labeled peaks	532 nm[a]	355 nm[a]	266 nm[a]
A	0.747[b]	0.799[c]	0.809[c]
X	1.297[b]	1.234[c]	1.279[c]
X′	1.407[b]	-	-
X″	1.476[b]	-	-
B	2.097[b]	2.131[c]	2.139[c]
C	-	2.737[b]	2.780[b]

[a]The photon wavelength used in each case to collect the spectrum. [b]The EBE values correspond to the intensity maxima for each peak. [c]The approximate peak position.

The electronic ground state for $HThO^-$ is the $1^1A'$ state, and the electronic ground state for HThO is the $1^2A'$ state. As shown in Table 1, the photodetachment of $HThO^-$ that results in HThO involves detachment of an 8a′ electron. Since the molecular orbital 8a′ receives most of its contribution from the Th 7s orbital, the detachment reduces the repulsion between the Th−H and Th−O bonding orbitals and hence shortens the Th−O bond by 0.03 Å and the Th−H bond by as much as 0.07 Å. The computed equilibrium structures and electronic energies are summarized in Figure 3. The relativistic coupled-cluster Th−H and Th−O bond lengths of 2.099 Å and 1.864 Å and H−Th−O bond angle of 105.7° for HThO compare reasonably well with previous DFT results of 2.054 Å, 1.869 Å, and 100.2°, respectively.[11] The present coupled-cluster results are expected to be of higher quality than previous DFT ones. We note that the DFT Th−H and Th−O bond lengths of 2.034 and 1.820 Å for the $HThO^+$ cation are shorter than those in the neutral molecule.[17] This may indicate that a removal of a Th 7s electron in HThO further shortens the bond lengths, which is consistent with the present observation that the bond lengths of HThO are shortened compared to $HThO^-$ with removal of a Th 7s electron.

The electronic energy difference between the $1^2A'$ state of HThO in its equilibrium geometry and the $1^1A'$ state of $HThO^-$ in its equilibrium geometry is calculated to be 1.23 eV. This together with the net zero-point vibrational correction of ∼0.03 eV, deduced from the harmonic vibrational frequencies in Table 3, leads to a computed adiabatic electron affinity, EA_a, of 1.26 eV, which is in good agreement with the measured value of EBE = 1.297 eV for feature, X, seen in Figure 2a and Table 2.

Figure 4 presents the vibrationally resolved photoelectron spectrum of $HThO^-$ (peaks, X, X′, and X″), measured with 532 nm photons along with the computational simulation of those peaks. Not only does the profile of the stimulated spectrum resemble that of the experimental spectrum, but the computed vibrational energy spacings of 0.106 eV for Th═O stretching and 0.176 eV for Th−H stretching are in nearly quantitative agreement with the respective values of 0.110 eV and 0.179 eV, measured in the photoelectron spectrum of $HThO^-$. These values are in accordance with Th═O and Th−H stretching frequencies of 0.105 and 0.176 eV, obtained via the combination of matrix-infrared spectroscopy and relativistic calculations.[11,12] The excellent agreement between experiment and theory firmly establishes feature, X, as the origin transition from the ground electronic state of $HThO^-$ to the ground electronic state of HThO. With this additional

https://dx.doi.org/10.1021/acs.jpca.0c11539
J. Phys. Chem. A 2021, 125, 1903−1909

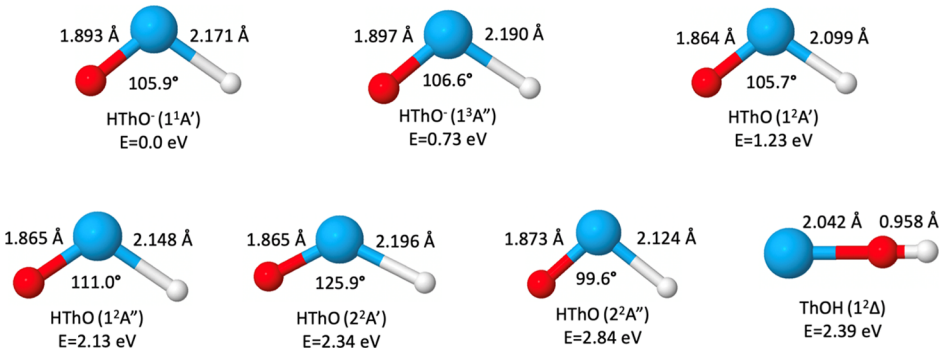

Figure 3. Computed equilibrium structures and electronic energies for low-lying electronic states of $HThO^-$, HThO, and ThOH.

Table 3. Harmonic Vibrational Frequencies (cm^{-1}) of the Electronic Ground States of $HThO^-$ and HThO Computed at the SFX2C-1e-CCSD(T)/Cc-pVTZ Level of Theory

	$HThO^-$ $1^1A'$	HThO $1^2A'$
H−Th−O bending	374	378
Th−O stretching	811	860
Th−H stretching	1259	1446

evidence, the adiabatic electron affinity (EA_a) of HThO is determined to be 1.297 ± 0.035 eV.

In addition to the origin-containing vibrational progression (observed as peaks X, X′, and X″), we now consider the nature of peaks A, B, and C in the photoelectron spectra of $HThO^-$ (Figure 2). Peak A is a low intensity feature located at EBE = 0.747 eV. This broad, weak peak is likely due to a small amount of ThO^- in the ion beam due to mass leakage (see Figure 1). The spectral position of this feature is consistent with the previously measured, ground state ThO^- → ground state ThO photodetachment transition at EBE ∼ 0.7 eV.[37] Both peaks B and C likely correspond to transitions from the ground electronic state of $HThO^-$ to an electronically excited state of the neutral HThO. These photoelectron spectral features are located at EBE values of ∼2.1 and ∼2.7 eV, respectively. Our calculations found that the vertical electronic energies for transitions from the $HThO^-$ $1^1A'$ state to the $1^2A''$, $2^2A'$, and $2^2A''$ excited electronic states of HThO are 2.15, 2.47, and 2.85 eV, respectively (see Table 1). Thus, transitions to these final (neutral) states are expected to contribute to features, B and C, in the range, EBE = 2.0−3.0 eV. Peak C is mostly likely due to the $1^1A'$ → $2^2A''$ anion to neutral transition. Nevertheless, the broad profiles of these two features insinuate underlying spectral complexity. The leading configuration of these three neutral states differ from that of the $1^1A'$ state of $HThO^-$ by more than one electron. Some of the intensities in these transitions may tentatively be attributed to strong electron correlation in the $1^1A'$ state of $HThO^-$. Similar observations of multiple electron processes have been reported for other heavy-metal-containing molecules, including ThO^-.[37]

The first excited state of $HThO^-$, that is, $1^3A''$, is predicted to lie 0.73 eV above the $HThO^-$ ground state, $1^1A'$. However, the $1^3A''$ state is unlikely to be significantly populated in our anion source, and the lifetime of the $1^3A''$ is short relative to production in the anion source and photodetachment. If the

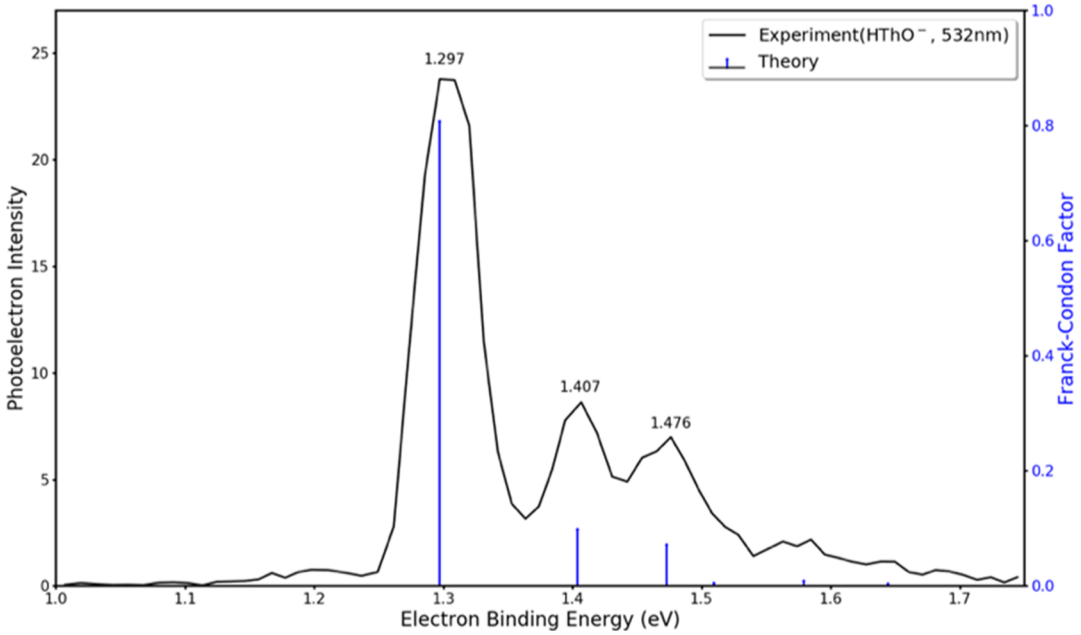

Figure 4. Photoelectron spectrum of $HThO^-$ collected with 532 nm wavelength photons of an Nd:YAG laser compared with the computational simulation. The computed electronic spectrum is blue-shifted by 0.03 eV to account for the net zero-point vibrational correction.

https://dx.doi.org/10.1021/acs.jpca.0c11539
J. Phys. Chem. A 2021, 125, 1903−1909

$1^3A''$ state of the anion was to have met these challenges, it would have produced an observed transition at EBE ~ 2.0/2.1 eV. We mention this outlying possibility only because there are very weak vibrational hot bands at EBE = 1.20 eV and 1.17 eV in the photoelectron spectrum of $HThO^-$ in Figures 2a and 4, implying that the nascent $HThO^-$ anions were not completely cold.

Despite the absence of computational or experimental evidence of the formation of the anion, $ThOH^-$, our theoretical results show that the neutral thorium hydroxide isomer, ThOH, lies around 2.39 eV above the $1^1A'$ ground state of $HThO^-$, as shown in Figure 3. Since photodetachment is a vertical ultra-fast process, there would not have been time for HThO neutral products of photodetachment to have isomerized into ThOH. Forming the ThOH isomer from HThO would involve the breaking and reforming of bonds. Although the Th−O−H atomic connectivity of ThOH no doubt occurs on the potential energy surfaces of the neutral photodetachment products, the ThOH potential must be well far from that of HThO and thus is not accessible by photodetachment.

Orbital Analysis. Orbitals 2a″ and 6a′ represent Th−O bonding orbitals (Figure 5). These orbitals are largely

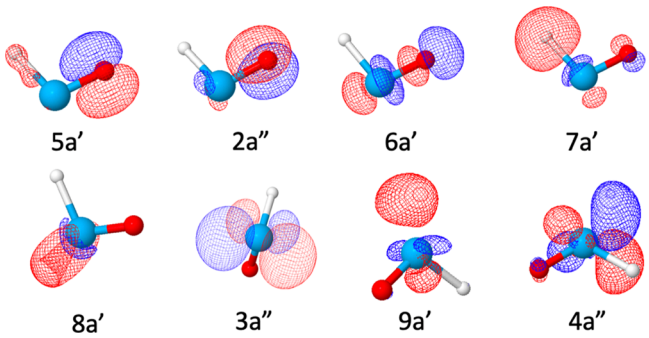

Figure 5. Valence HF orbitals of $HThO^-$ involved in photodetachment processes or bonding.

transferable from ThO (or ThO^-) to HThO (or $HThO^-$). Orbital 7a′ appears to be responsible for the Th−H bond and consists of around 70% H 1s orbital and 30% Th 6d orbital. These three orbitals are doubly occupied in $HThO^-$ and in all electronic states of HThO studied here. Calculations show that detachment of an electron from these orbitals requires photon energies higher than 4 eV. Since the electronegative oxygen atom in ThO^- already has an appreciable negative charge, it is less energetically favorable for hydrogen to donate its electron to oxygen to form an O−H bond. The addition of hydrogen to ThO^- thus favors the thorium site, in which hydrogen atom plays the role as an acceptor of an electron from Th 6d orbitals.

As shown in Figure 5, orbital 8a′ is by and large a polarized Th 7s orbital and is doubly occupied in $HThO^-$. Detachment of an electron in this orbital leads to the electronic ground state of the neutral molecule. The detachment to generate the $1^2A''$, $2^2A'$, or $2^2A''$ state of HThO involves detachment of an 8a′ electron accompanied by an excitation from the 8a′ orbital to the 3a″, 9a′, or 4a″ orbital, respectively, which as shown in Figure 5 receives most of the contributions from the Th 6d orbitals.

CONCLUSIONS

In this paper, we present a combined experimental and high-level computational study of the connectivity and electronic structures of the HThO molecule and the $HThO^-$ anion. The present experiment uses the reaction of ThO^- with H_2 gas to produce $HThO^-$. Since the oxygen atom in ThO^- already possesses a substantial negative charge, it is not energetically favorable for hydrogen to donate an electron to oxygen to form an O−H bond and $ThOH^-$. Instead, a hydrogen atom accepts an electron from the Th 6d orbital to form $HThO^-$. Photodetachment of the ground state of anion $HThO^-$ ($1^1A'$) to form the electronic ground state of the neutral HThO ($1^2A''$) ejects a thorium 7s electron. This reduces the repulsion with the Th−H and Th−O bonding orbitals and causes their bond lengths to shorten. The adiabatic electron affinity of HThO is accurately determined by resolving the vibrational progression for this transition. In addition, transitions from the ground state of $HThO^-$ to electronically excited states of HThO are characterized to provide valuable information about the electronic structure of HThO.

AUTHOR INFORMATION

Corresponding Authors

Lan Cheng − *Department of Chemistry, Johns Hopkins University, Baltimore, Maryland 21218, United States;* orcid.org/0000-0003-1165-9559; Email: lcheng24@jhu.edu

Kit H. Bowen − *Department of Chemistry, Johns Hopkins University, Baltimore, Maryland 21218, United States;* orcid.org/0000-0002-2858-6352; Email: kbowen@jhu.edu

Authors

Mary Marshall − *Department of Chemistry, Johns Hopkins University, Baltimore, Maryland 21218, United States;* orcid.org/0000-0001-6614-1963

Zhaoguo Zhu − *Department of Chemistry, Johns Hopkins University, Baltimore, Maryland 21218, United States;* orcid.org/0000-0002-4395-9102

Junzi Liu − *Department of Chemistry, Johns Hopkins University, Baltimore, Maryland 21218, United States*

Complete contact information is available at: https://pubs.acs.org/10.1021/acs.jpca.0c11539

Author Contributions

The experimental work was done at Johns Hopkins University by M.M. and Z.Z. K.H.B. supervised the experiments. The computational work was done at Johns Hopkins University by J.L. and L.C. The manuscript was written as a collaborative effort.

Notes

The authors declare no competing financial interest.

ACKNOWLEDGMENTS

The experimental portion of this material is based upon work supported by the U.S. Department of Energy (DOE), Office of Science, Office of Basic Energy Sciences, Heavy Element Chemistry program under Award Number, DE-SC0019317 (K.H.B.). The computational portion of this material is based upon work supported by the U.S. Department of Energy (DOE), Office of Science, Office of Basic Energy Sciences, under Award Number DE-SC0020317 (L.C.).

https://dx.doi.org/10.1021/acs.jpca.0c11539
J. Phys. Chem. A 2021, 125, 1903−1909

ABBREVIATIONS

EAa	adiabatic electron affinity
DFT	density-functional theory
M	actinides
M′	group IV metals
PES	anion photoelectron spectroscopy
Nd:YAG	neodymium-doped yttrium aluminum garnet
EBE	electron binding energy
EKE	electron kinetic energy
UHP	ultra-high purity
CFOUR	coupled-cluster techniques for Computational Chemistry
CCSD(T)	coupled-cluster singles and doubles with non-iterative triples
SFX2C-1e	spin-free exact two-component theory in its one-electron variant
cc-pVTZ	correlation-consistent polarized valence triple zeta
EOMEA-CCSD	equation-of-motion electron attachment coupled-cluster singles and doubles
FC	Franck−Condon
eV	electron volt

REFERENCES

(1) Morss, L. R. *The Chemistry of the Actinide and Transactinide Elements*; Springer: Netherlands, 2010.

(2) Lung, M.; Gremm, O. Perspectives of the Thorium Fuel Cycle. *Nucl. Eng. Des.* **1998**, *180*, 133−146.

(3) Lombardi, C.; Luzzi, L.; Padovani, E.; Vettraino, F. Thoria and Inert Matrix Fuels for a Sustainable Nuclear Power. *Prog. Nucl. Energy* **2008**, *50*, 944−953.

(4) Bae, K.-M.; Kim, M.-H. Core Design for Heterogeneous Thorium Fuel Assemblies for PWR (I)-Nuclear Design and Fuel Cycle Economy. *Nucl. Eng. Technol.* **2005**, *37*, 91−100.

(5) Ekberg, C.; Albinsson, Y.; Comarmond, M. J.; Brown, P. L. Studies on the Complexation Behavior of Thorium (IV). 1. Hydrolysis Equilibria. *J. Solution Chem.* **2000**, *29*, 63−86.

(6) Engkvist, I.; Albinsson, Y. Hydrolysis Studies of Thorium Using Solvent Extraction Technique. *Radiochim. Acta* **1992**, *58*−*59*, 109−112.

(7) Moulin, C.; Amekraz, B.; Hubert, S.; Moulin, V. Study of Thorium Hydrolysis Species by Electrospray-Ionization Mass Spectrometry. *Anal. Chim. Acta* **2001**, *441*, 269−279.

(8) Baes, C. F.; Meyer, N. J.; Roberts, C. E. The Hydrolysis of Thorium(IV) at 0 and 95°. *Inorg. Chem.* **1965**, *4*, 518−527.

(9) Kafle, A.; Armentrout, P. B. Mechanism and Energetics of the Hydrolysis of Th^+ to form $Th(OD)_3^+$: Guided Ion Beam and Theoretical Studies of ThO^+, ThO_2^+, and $OThOD^+$ reacting with D_2O. *J. Phys. Chem. A* **2019**, *123*, 5893−5905.

(10) Kafle, A.; Nwokolo, C.; Sanchez, L.; Armentrout, P. B. Threshold Collision-Induced Dissociation of Hydrated Th(IV) Trihydroxide Cation: Experimental and Theoretical Investigation of the Binding Energies for $Th(OH)_3^+(H_2O)_n$ Complexes (n = 1-4). *J. Phys. Chem. A* **2020**, *124*, 3090−3100.

(11) Liang, B.; Andrews, L.; Li, J.; Bursten, B. E. Experimental and Theoretical Studies of the Products of Laser-Ablated Thorium Atom Reactions with H_2O in Excess Argon. *J. Am. Chem. Soc.* **2002**, *124*, 6723−6733.

(12) Wang, X.; Andrews, L. Infrared Spectra and Structures of the $Th(OH)_2$ and $Th(OH)_4$ Molecules. *Phys. Chem. Chem. Phys.* **2005**, *7*, 3834−3838.

(13) Cox, R. M.; Armentrout, P. B. Activation of Water by Thorium Cation: A Guided Ion Beam and Quantum Chemical Study. *J. Am. Soc. Mass Spectrom.* **2019**, *30*, 1835−1849.

(14) Santos, M.; Marçalo, J.; Pires de Matos, A.; Gibson, J. K.; Haire, R. G. Gas-Phase Oxidation Reactions of Neptunium and Plutonium Ions Investigated via Fourier Transform Ion Cyclotron Resonance Mass Spectrometry. *J. Phys. Chem. A* **2002**, *106*, 7190−7194.

(15) Cornehl, H. H.; Wesendrup, R.; Diefenbach, M.; Schwarz, H. A Comparative Study of Oxo-Ligand Effects in the Gas-Phase Chemistry of Atomic Lanthanide and Actinide Cations. *Chem.—Eur. J.* **1997**, *3*, 1083−1090.

(16) Gibson, J. K.; Haire, R. G.; Santos, M.; Marçalo, J.; Pires de Matos, A. Oxidation Studies of Dipositive Actinide Ions, An^{2+} (An = Th, U, Np, Pu, Am) in the Gas Phase: Synthesis and Characterization of the Isolated Uranyl, Neptunyl, and Plutonyl Ions $UO_2^{2+}(g)$, $NpO_2^{2+}(g)$, and $PuO_2^{2+}(g)$. *J. Phys. Chem. A* **2005**, *109*, 2768−2781.

(17) Mazzone, G.; Michelini, M. D. C.; Russo, N.; Sicilia, E. Mechanistic Aspects of the Reaction of Th^+ and Th^{2+} with Water in the Gas Phase. *Inorg. Chem.* **2008**, *47*, 2083−2088.

(18) del Carmen Michelini, M.; Russo, N.; Sicilia, E. How Can Uranium Ions (U^+, U^{2+}) Activate the O-H Bond of Water in the Gas Phase? *Angew. Chem.* **2006**, *118*, 1113−1117.

(19) Delegard, C. H.; Schmidt, A. J. *Uranium Metal Reaction Behavior in Water, Sludge, and Grout Matrices*. Pacific Northwest National Laboratory, 2008.

(20) Haschke, J. M. *Reactions of Plutonium and Uranium with Water: Kinetics and Potential Hazards*; Los Alamos National Laboratory, 1995.

(21) Shao, L.; Zhang, L.; Chen, M.; Lu, H.; Zhou, M. Reactions of Titanium Oxides with Water Molecules. A Matrix Isolation FTIR and Density Functional Study. *Chem. Phys. Lett.* **2001**, *343*, 178−184.

(22) Gerhards, M.; Thomas, O. C.; Nilles, J. M.; Zheng, W.-J.; Bowen, K. H. Cobalt-Benzene Cluster Anions: Mass Spectrometry and Negative Ion Photoelectron Spectroscopy. *J. Chem. Phys.* **2002**, *116*, 10247−10252.

(23) Ho, J.; Ervin, K. M.; Lineberger, W. C. Photoelectron Spectroscopy of Metal Cluster Anions: Cu_n^-, Ag_n^-, and Au_n^-. *J. Chem. Phys.* **1990**, *93*, 6987−7002.

(24) Matthews, D. A.; Cheng, L.; Harding, M. E.; Lipparini, F.; Stopkowicz, S.; Jagau, T.-C.; Szalay, P. G.; Gauss, J.; Stanton, J. F. Coupled-Cluster Techniques for Computational Chemistry: The CFOUR Program Package. *J. Chem. Phys.* **2020**, *152*, 214108.

(25) CFOUR. Coupled-Cluster Techniques for Computational Chemistry, a quantum-chemical program package by Stanton, J. F.; Gauss, J.; Cheng, L.; Harding, M. E.; Matthews, D. A.; Szalay, P. G.; with contributions from Auer, A. A.; Bartlett, R. J.; Benedikt, U.; Berger, C.; Bernholdt, D. E.; Bomble, Y. J.; Christiansen, O.; Engel, F.; Faber, R.; Heckert, M.; Heun, O.; Hilgenberg, M.; Huber, C.; Jagau, T.-C.; Jonsson, D.; Juselius, J.; Kirsch, T.; Klein, K.; Lauderdale, W. J.; Lipparini, F.; Metzroth, T.; Mück, L. A.; O'Neill, D. P.; Price, D. R.; Prochnow, E.; Puzzarini, C.; Ruud, K.; Schiffmann, F.; Schwalbach, W.; Simmons, C.; Stopkowicz, S.; Tajti, A.; Vaźquez, J.; Wang, F.; Watts, J. D.; and the integral packages MOLECULE (Almlöf, J.; Taylor, P. R.), PROPS (Taylor, P. R.), ABACUS (Helgaker, T.; Jensen, H. J. A.; Jørgensen, P.; Olsen, J.), and ECP routines by Mitin, A. V.; van Wüllen, C. For the current version, see http://www.cfour.de.

(26) Watts, J. D.; Gauss, J.; Bartlett, R. J. Coupled-cluster Methods with Noniterative Triple Excitations for Restricted Open-Shell Hartree−Fock and Other General Single Determinant Reference Functions. Energies and Analytical Gradients. *J. Chem. Phys.* **1993**, *98*, 8718.

(27) Stanton, J. F.; Gauss, J. Analytic Energy Gradients for the Equation-of-Motion Coupled-Cluster Method: Implementation and Application to the HCN/HNC System. *J. Chem. Phys.* **1994**, *100*, 4695.

(28) Cheng, L.; Gauss, J. Analytic Energy Gradients for the Spin-Free Exact Two-Component Theory using an Exact Block Diagonalization for the One-Electron Dirac Hamiltonian. *J. Chem. Phys.* **2011**, *135*, 084114.

(29) Stanton, J. F.; Lopreore, C. L.; Gauss, J. The Equilibrium Structure and Fundamental Vibrational Frequencies of dioxirane. *J. Chem. Phys.* **1998**, *108*, 7190.

https://dx.doi.org/10.1021/acs.jpca.0c11539
J. Phys. Chem. A 2021, 125, 1903−1909

(30) Matthews, D. A.; Vázquez, J.; Stanton, J. F. Calculated Stretching Overtone Levels and Darling- Dennison Resonances in Water: A triumph of Simple Theoretical Approaches. *Mol. Phys.* **2007**, *105*, 2659−2666.
(31) Raghavachari, K.; Trucks, G. W.; Pople, J. A.; Head-Gordon, M. A Fifth-Order Perturbation Comparison of Electron Correlation Theories. *Chem. Phys. Lett.* **1989**, *157*, 479−483.
(32) Dyall, K. G. Interfacing relativistic and nonrelativistic methods. IV. One- and Two-Electron Scalar Approximations. *J. Chem. Phys.* **2001**, *115*, 9136−9143.
(33) Liu, W.; Peng, D. Exact Two-Component Hamiltonians Revisited. *J. Chem. Phys.* **2009**, *131*, 031104.
(34) Peterson, K. A. Correlation Consistent Basis Sets for Actinides. I. The Th and U Atoms. *J. Chem. Phys.* **2015**, *142*, 074105.
(35) Dunning, T. H. Gaussian Basis Sets for Use in Correlated Molecular Calculations. I. The Atoms Boron through Neon and Hydrogen. *J. Chem. Phys.* **1989**, *90*, 1007−1023.
(36) Nooijen, M.; Bartlett, R. J. Equation of Motion Coupled Cluster Method for Electron Attachment. *J. Chem. Phys.* **1996**, *102*, 3629.
(37) Li, Y.; Zou, J.; Xiong, X.-G.; Su, J.; Xie, H.; Fei, Z.; Tang, Z.; Liu, H. Probing Chemical Bonding and Electronic Structures in ThO^- by Anion Photoelectron Imaging and Theoretical Calculations. *J. Phys. Chem. A* **2017**, *121*, 2108−2113.

https://dx.doi.org/10.1021/acs.jpca.0c11539
J. Phys. Chem. A 2021, 125, 1903−1909